Zinc-Ion Batteries | **Hot Paper**

High-Capacity and Long-Life Cathode Constructed Solely by Carbon Dots for Aqueous Zinc-Ion Batteries

Tian-Bing Song, Qian-Li Ma, Bao-Juan Wang, Xi-Rong Zhang, Yong-Gang Wang,*
and Huan-Ming Xiong*

Abstract: Carbon dots (CDs) have been explored widely in the electrochemistry field, owing to their unique structures and rich properties. However, in the reported devices, such as batteries and supercapacitors, CDs are always used as additives to modify the electrodes or regulate the electrolytes because they have been regarded as inert and low-capacity materials all along. Here, for the first time, *o*-phenylenediamine derived CDs are selected as the only protagonist to construct cathode materials for aqueous zinc-ion batteries (ZIBs). Such CDs (p-CDs) have a special π-conjugated phenazine-based structure, with carbon cores for electrical conductivity and active sites for embedding Zn^{2+} and H^+. The p-CDs solely constructed cathode material delivers a superior capacity of 290 mAh g^{-1} at 0.1 A g^{-1} and a decent capacity of 103 mAh g^{-1} at an ultra-high current density of 10 A g^{-1}, as well as an ultrahigh ion diffusion coefficient of $10^{-8} \sim 10^{-7}$ cm^2 s^{-1}. The p-CDs assembled ZIBs exhibit a stable long-term cycling, retaining 87.4% of the original capacity after 10 000 cycles. Various characterizations and theoretical calculations prove that the electron-deficient N as the active sites on p-CDs can embed/release Zn^{2+} and H^+ reversibly.

Introduction

In the past 20 years, carbon dots (CDs), due to their unique structures and abundant properties, have been investigated extensively in many fields, including fluorescent probes, LEDs, catalysts, batteries, and supercapacitors, *etc.*[1–3] Recently, for modifying electrodes or regulating electrolytes, CDs are introduced to aqueous zinc-ion batteries (ZIBs),[4] which are competitive energy storage devices owing to their low-cost, abundant resources, environmental benignity, and

operating safety. After coating or deposition, CDs are able to protect Zn anodes through inhibiting interfacial side reactions, dendrite growth, and electrolyte corrosion.[5] Besides, the well-designed and doped CDs are added into the ZnSO₄-based electrolyte, which can modulate Zn^{2+} ion solvation structures, facilitate the preferential Zn^{2+} ion flux, and induce the homogeneous Zn nucleation and deposition, so as to achieve long-term stable cycles.[6] On the cathode side, CDs mainly emerge in the composites with other active materials, such as manganese oxides, vanadium oxides, polyaniline, and Prussian blue analogs.[7–10] CDs play different roles in these nanocomposites, such as regulating materials structure and morphology, building pores and channels, expanding the surface areas, accelerating interfacial ion transport, and improving the electrical conductivity. By far, CDs have never been used alone to construct cathode materials for ZIBs, as well as other electrodes in various electrochemical energy storage devices to our knowledge, because most CDs have good solubility in aqueous or organic electrolytes, and they are inert during electrochemical reactions.

In fact, CDs are not only carbon nanoparticles but also organic–inorganic hybrid nanomaterials. A main type of CDs is named carbonized polymer dots, which are synthesized from some organic molecules, via polymerization and carbonization in one pot reaction.[11,12] They can be designed meticulously and synthesized precisely, to meet the requirements of electrode materials for ZIBs. These requirements include appropriate electronic conductivities, abundant active sites for Zn^{2+} or H^+ insertion/extraction, suitable redox potentials, long stability during cycles, rich resources, environmental friendliness, *etc.*[13,14] Carbon dots can meet most of the above requirements because they are naturally stable, conductive, cheap, and environmental benign.[15,16] Hence, the challenge of this research focuses on the mechanism of Zn^{2+} or H^+ insertion/extraction on the CDs constructed materials, which determines the capacity of such cathode and the cycling performance of the assembled ZIBs.

In this work, *o*-phenylenediamine was selected to synthesize CDs hydrothermally with a small amount of hydrochloric acid. The obtained p-CDs have a π-conjugated phenazine structure and plenty of C=N groups. Such a structure allows Zn^{2+} and H^+ insertion/extraction through the redox pseudocapacitance mechanisms, which are proved by a series of in situ and ex situ characterizations and also predicted by theoretical calculations. The conjugated carbon bonds facilitate electronic conduction, while the surface groups and channels accelerate Zn^{2+} and H^+ diffusion, achieving a fast

[*] Dr. T.-B. Song, Q.-L. Ma, B.-J. Wang, X.-R. Zhang, Prof. Y.-G. Wang,
Prof. H.-M. Xiong
Department of Chemistry, Shanghai Key Laboratory of
Electrochemical and Thermochemical Conversion for Resources
Recycling, Fudan University, Shanghai 200438, China
E-mail: ygwang@fudan.edu.cn
hmxiong@fudan.edu.cn

☐ Additional supporting information can be found online in the
Supporting Information section
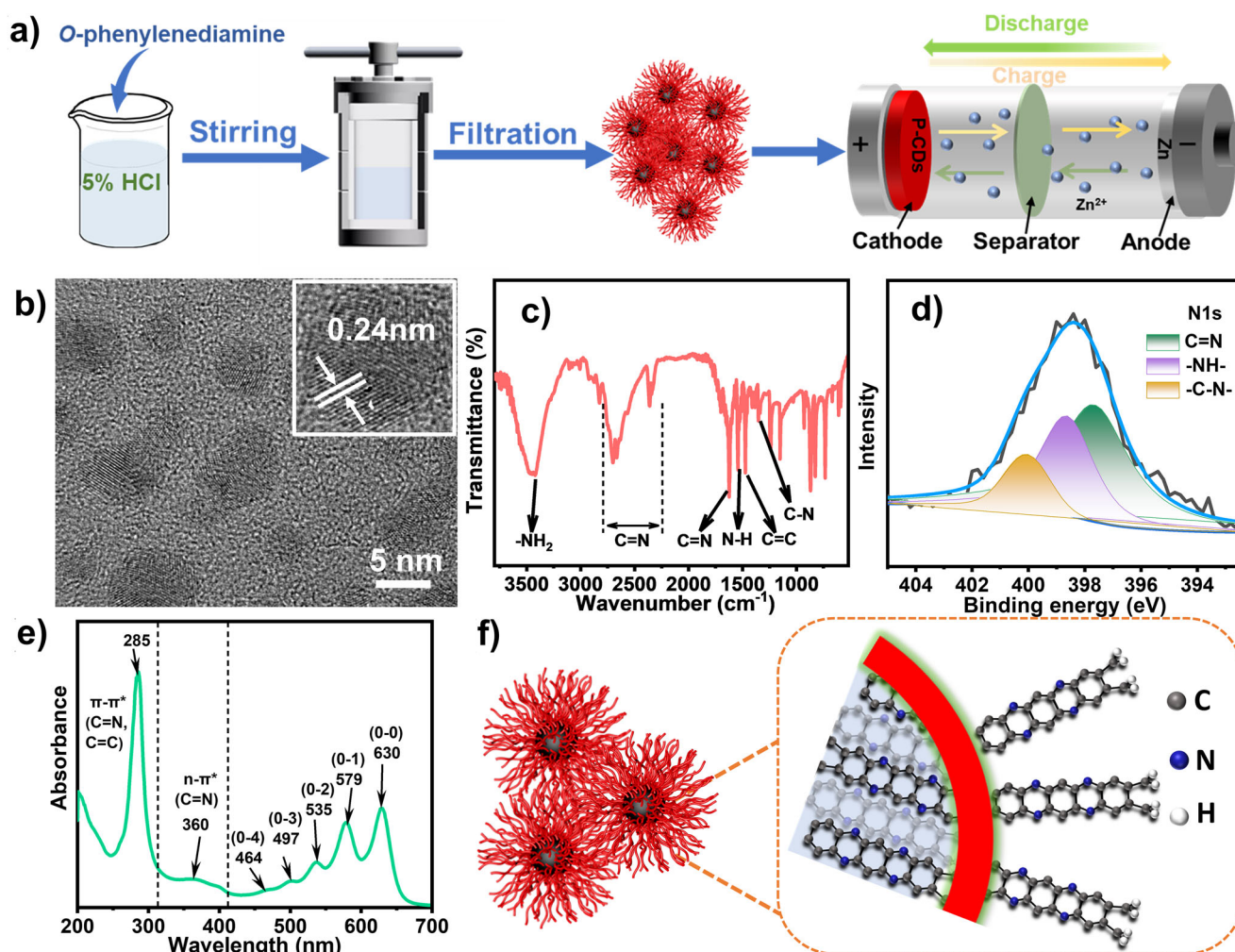
Figure 1. a) Schematic illustration of p-CDs synthesis and application. b) TEM image and the inset HRTEM image of p-CDs. c) FITR spectra, d) high resolution XPS for N 1s, and e) absorption spectrum of p-CDs. f) A schematic structure for p-CDs.

redox kinetics. As a result, the p-CDs deliver a superior capacity of 290 mAh g^{-1} at a normal current density 0.1 A g^{-1} and a decent capacity of 103 mAh g^{-1} at an ultra-high current density of 10 A g^{-1}, respectively. After 10 000 cycles in ZIBs, the capacity still retains 87.4% of the original. This work confirms that the well-designed CDs can act as cathode materials solely for high energy storage with long lifespan.

Results and Discussion

The p-CDs are synthesized hydrothermally from *o*-phenylenediamine and hydrochloric acid, purified by washing with water, and then used as the active materials for ZIBs (Figure 1a). This route provides sufficient products to assemble batteries with a large scale, a low cost, and a facile operation. Both the TEM and HRTEM images in Figures 1b and S1 show that p-CDs are monodispersed nanoparticles with diameters of 5 ∼ 8 nm. HRTEM images clearly reveal two lattice distances of 0.21 and 0.24 nm, corresponding to the graphite lattice planes of (100) and (1120) respectively.[17] In Figure 1c, the FTIR peaks at 1542 and 3447 cm^{-1} are assigned

to N–H and −NH$_2$ groups respectively, while the peaks at 2290∼2790 and 1624 cm^{-1} are assigned to the stretching vibrations of C═N groups. The absorption band at 1353 cm^{-1} originates from the bending vibration of C−N, and the peak at 1475 cm^{-1} corresponds to the C═C bond.[18] The XPS analyzes also confirm the above chemical bonds in p-CDs (Figures 1d and S2). The high-resolution XPS deconvolution of N 1s (Figure 1d) verifies the existence of C═N (397.6 eV), −C−N− (398.71 eV) and −NH− (400.2 eV), while the C 1s spectrum (Figure S2b) contains the signals of sp^2 C (C═C at 284.8 eV, C═N at 288.1 eV) and sp^3 C (C−C at 285.2 eV, C−N at 286.2 eV), respectively.[19,20] Both FTIR spectra and XPS analyses prove p-CDs have plenty of C═N groups.

The UV–vis spectra of p-CDs can be separated into three regions according to the earlier research (Figure 1e).[19–22] The absorption at 285 nm is assigned to the π−π* transition (C═C and C═N), and the absorption at ∼360 nm is assigned to the n–π* transition (C═N).[20] Particularly, the absorption at 400∼700 nm can be defined as vibronic overtone bands with the (0–0) transition at 630 nm and with a decrease in energy difference between two overtone bands, which strongly proves that p-CDs possess π-conjugated aromatic
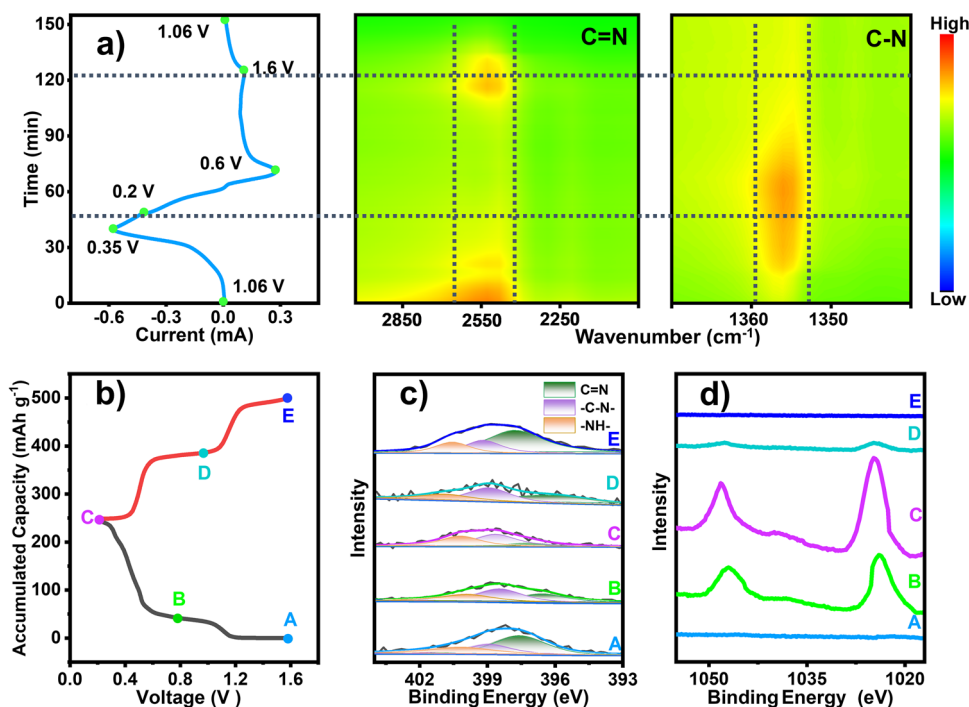
Figure 2. The energy storage mechanism of p-CDs in 2 M Zn(OTf)$_2$ electrolyte. a) The 2D color-filled contour plots of the in situ ATR-FTIR spectra for the p-CDs electrode during a CV test at a scan rate of 0.5 mV s^{-1}. b) The discharge/charge curve of Zn∥p-CDs battery at 0.1 A g^{-1}. At the marked points in discharge/charge curves, five samples A ∼ E are taken out from p-CDs electrodes and measured by XPS spectra of c) N 1s and d) Zn 2p, respectively.

structures.[21,22] The ethanol solution of p-CDs is blue in daylight and emit red fluorescence under UV light (Figure S3). Its emission spectra also have three peaks at about 600, 660 and 710 nm, respectively, and these peak positions do not shift as the excitation wavelength varies from 450 to 570 nm, in accord with those *o*-phenylenediamine derived CDs in the literature.[23] According to the above analyzes, as well as the p-CDs synthesis and those previous reports,[18–20] our p-CDs are made up of π-conjugated phenazine-based structures (Figure 1f), which can provide active sites for zinc ion storage. Moreover, the specific surface area of CDs is measured to be 14.04 m^2 g^{-1} by the Brunauer–Emmett–Teller (BET) method (Figure S4a). The thermogravimetric (TGA) curve in Figure S4b shows two main regions of weight loss. One is at around 300 ∼ 400 °C due to the decomposition of surface groups, while the other is at around 450 ∼ 650 °C that can be regarded as decomposition of the carbon cores. Obviously, the carbon cores are the main component of p-CDs. In addition, the electrical conductivity of our CDs reaches 0.0128 S cm^{-1} at room temperature (Figure S4c), which is higher than those of most polymers and organic materials.[24,25]

The electrochemical reaction process of p-CDs is also manifested in the variation of their unique optical features. ATR-FTIR spectra were monitored in situ to analyze the structure change of p-CDs during a CV test at a scan rate of 0.5 mV s^{-1}. In Figure 2a, the absorption peaks of C=N bond at 2520 cm^{-1} decreases gradually during the negative sweep step (from 1.06 to 0.2 V), which is ascribed to the coordination reaction of C=N bond with H$^+$ in the p-CDs electrode. On the contrary, the absorption peak at 1355 cm^{-1} increases,

owing to the augment of —C—N— bond. In the following oxidation process (from 0.2 to 1.6 V), the absorption peak of C=N bond increases gradually, which illustrates the release of H$^+$ from p-CDs, corresponding the decrease of —C—N— bonds. In the UV–vis spectra of p-CDs at different states (Figure S5), the peaks at 285 nm corresponding to the C=C network do not change significantly during charge/discharge cycles. In contrast, the absorption peaks at 360 nm of C=N bond disappear at the fully charged state and reappear at the discharged state, confirming the high reversibility of the p-CDs electrode. In addition, the absorption peaks at 540, 570 and 630 nm show noticeable changes, which can be ascribed to conjugated phenazine rings during the H$^+$ insertion/extraction in the p-CDs material.

Meanwhile, XPS measurements are carried out to explore the energy storage mechanism of p-CDs in ZIBs at the selected states A ∼ E of discharge/charge cycles in Figure 2b. The XPS curves (Figure 2c) of these five samples can be deconvoluted into three peaks, respectively. Among them, the ratio of C=N groups reduces during the discharge process (from A to C), while the signals of —C—N— and —NH— components enhance gradually. This suggests that the C=N groups of p-CDs are reduced to —C—N— species during the discharge process, and in the meantime, more —NH— groups form to coordinate with H$^+$. In the subsequent charge process from C to E, the peak ratios of —C—N— and —NH— groups decrease gradually, and the C=N component recovers again, indicating that H$^+$ are extracted from p-CDs electrode. In the XPS data (Figure 2d), Zn 2p peaks at 1021.8 and 1044.8 eV appear in the discharged state and almost disappear after the
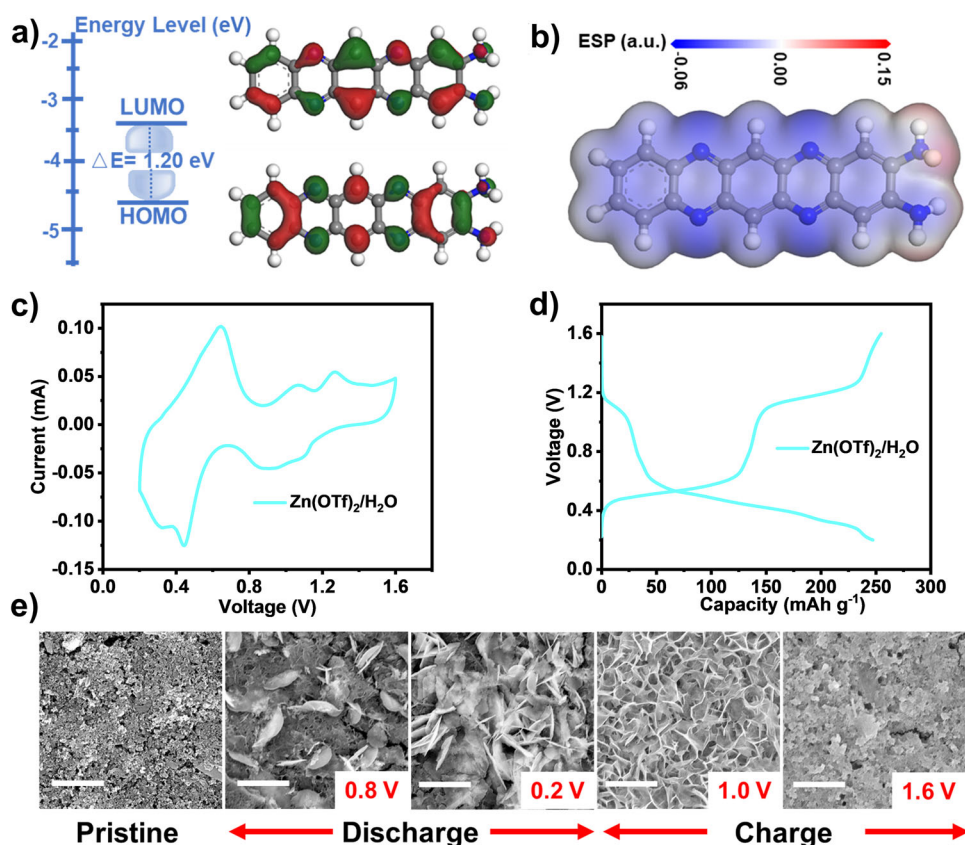
Figure 3. a) HOMO/LUMO energy levels and the energy gap (ΔE) calculated by a DFT method, b) MESP distribution on the van der Waals surface, c) CV curves of p-CDs measured at 0.1 mV s^{-1}, and d) charge/discharge curves of p-CDs mat 0.1 A g^{-1} in 2 M Zn(OTf)$_2$/H$_2$O electrolyte. e) SEM images of the samples at different charged/discharged states. The white bars represent 5 μm.

battery is charged to 1.6 V. This result confirms that both Zn^{2+} and H$^+$ ions can insert into p-CDs during discharging and leave from p-CDs during charging reversibly.

Since the p-CDs are derived from the phenazine-based molecular structure, the phenazine is selected as the smallest unit in the calculation process. DFT calculations are conducted to disclose the effect of the phenazine-based molecular structure on the p-CDs charge/discharge process. The calculation results show that the ΔE gap between HOMO and LUMO is 1.20 eV (Figure 3a), which is lower than those of most organic materials,[26–28] indicating that p-CDs have both good electrical conductivity and fast charge transfer ability. Normally, the molecular electrostatic potential (MESP) is employed to analyze the electrophilic and nucleophilic reaction active sites.[29] As for the phenazine-based molecular structure, N atoms are the active centers possibly due to their high electronegativity (Figure 3b). Therefore, N atoms sites with more negative electrostatic potential are more likely to bind Zn^{2+} or H$^+$, in accord with the results of the above measurements.

To determine the Zn^{2+} and H$^+$ embedding in p-CDs, CV and charged/discharged measurements are performed in different electrolytes, respectively, including 2 M Zn(OTf)$_2$/H$_2$O, 0.05 M H$_2$SO$_4$/H$_2$O, and 2 M Zn(OTf)$_2$/acetonitrile(ACN). As shown in the CV curves of p-CDs electrodes in different electrolytes, there are two reduction peaks at about 0.4 V

and 0.65~1.15 V in both Zn(OTf)$_2$/H$_2$O (Figure 3c) and Zn(OTf)$_2$/ACN (Figure S6a), corresponding to the Zn^{2+} intercalation. It is clear that the p-CDs electrode exhibits the higher capacity in Zn(OTf)$_2$/H$_2$O (Figure 3d) than it does in Zn(OTf)$_2$/ACN (Figure S6b). Although the charge/discharge curves of p-CDs in the aqueous electrolyte are similar with that in the organic electrolyte, the latter shows the higher platforms due to the different solvation structures of Zn^{2+}. Moreover, their dQ/dV curves are much different in Figure S7. Hence, it is necessary to distinguish the ion storage mechanisms in different electrolytes.

The electrochemical behaviors of the p-CDs electrode in the acidic electrolyte (0.05 M H$_2$SO$_4$ without Zn^{2+}) are investigated by a three-electrode system, using Hg/Hg$_2$SO$_4$ (soaked in the saturated K$_2$SO$_4$ solution) as the reference electrode (0.613 V vs. SHE) and Pt as the counter electrode because Zn is unstable in acidic solutions. As shown in Figure S8, the electrochemical measurement range is $-0.75 \sim 0.47$ V (vs. Hg/Hg$_2$SO4), which is transformed into the corresponding potential (vs. Zn^{2+}/Zn) on the upper horizontal axis. The CV and charge/discharge measurements are performed at a scan rate of 1 mV s^{-1} and a current density of 1 A g^{-1}. The CV curve shows two oxidation/reduction peaks in Figure S8a, while the p-CDs electrode delivers an initial discharge capacity of about 45 mAh g^{-1} at 1 A g^{-1} in Figure S8b. These results indicate that p-CDs have the
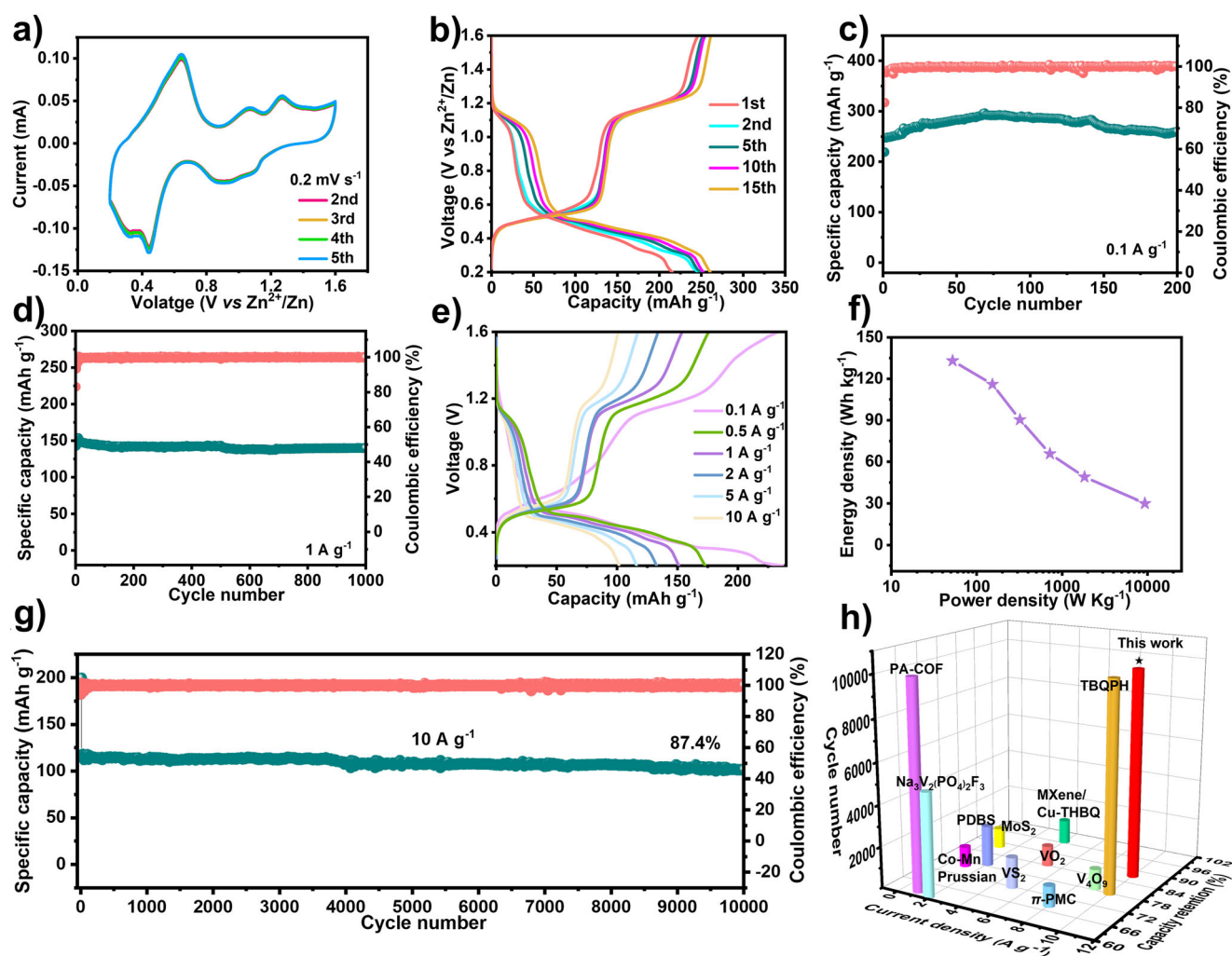
Figure 4. Electrochemical measurements of p-CDs electrodes. a) Cyclic voltammograms at a scan rate of 0.2 mV s^{-1}. b) Charge/discharge curves and c) Cycling performance at 0.1 A g^{-1} with good capacities (green) and excellent CE (red). d) Cycling performance at 1 A g^{-1} with good capacities (green) and excellent CE (red). e) Rate charge/discharge curves under different current densities, respectively. f) Ragone plots of the Zn∥p-CDs cell. g) Long cyclic stability at a high current density of 10 A g^{-1} with good capacities (green) and excellent CE (red). h) Comparison of our p-CDs cathode with those representative organic and inorganic ZIB cathodes in the literature.

ability to store H$^+$ in the acidic electrolyte. After shifting the CV curve to the weakly acidic condition (pH = 4.06, corresponding to the pH value of the Zn(OTf)$_2$/H$_2$O) according to the Nernst equation, the obtain CV curve in Figure S8a can overlap partly with that in Figure 3c, which means in the Zn(OTf)$_2$/H$_2$O electrolyte, the p-CDs can also store H$^+$.

In addition, the SEM images of p-CDs electrode at different charge/discharge states are listed in Figure 3e, which clearly show the flower-like Zn compounds emerge during discharging and disappear during charging. This further indicates that the H$^+$ and Zn^{2+} uptake/removal behaviors in the p-CDs, and these phenomena are consistent with the EDS mapping analyzes in Figure S9. Based on all these analyzes, we elucidate the electrochemical mechanism in this battery system that a highly reversible Zn^{2+} and H$^+$ insertion/extraction behavior occurs at the redox-active C=N groups of p-CDs.

The electrochemical properties of p-CDs were evaluated in detail through constant current charge and discharge tests.

The CV curves of the first five cycles overlap with each other (Figure 4a), affirming the good stability of p-CDs and the reversibility of the Zn^{2+} and H$^+$ insertion/extraction processes. Figure 4b show the galvanostatic charge/discharge curves in the aqueous electrolyte, which are tested at 0.1 A g^{-1} at a range of 0.2 ∼ 1.6 V (vs. Zn^{2+}/Zn). The p-CDs electrode displays remarkable capacity, stability, and reversibility, which delivers a capacity of 290 mAh g^{-1} at a current density of 0.1 A g^{-1} after the initial activation (Figure 4c). The improvement of the cycling performance of batteries at the initial stage is generally attributed to the electrochemical activation process. In contrast, the Coulombic efficiency (CE) of p-CDs in Zn(OTf)$_2$/ACN electrolyte is only about 80% (Figure S10), much lower than the CE (99%) in the aqueous electrolyte. This phenomenon is owing to the solubility of p-CDs in the organic electrolyte, which can be seen clearly in Figure S11a. In contrast, p-CDs are insoluble in the aqueous electrolyte, so the separator keeps white and clean after cycles in ZIBs (Figure S11b). Contact angles of the aqueous and

Angew. Chem. Int. Ed. **2025**, 64, e202503655 (5 of 8)

© 2025 Wiley-VCH GmbH
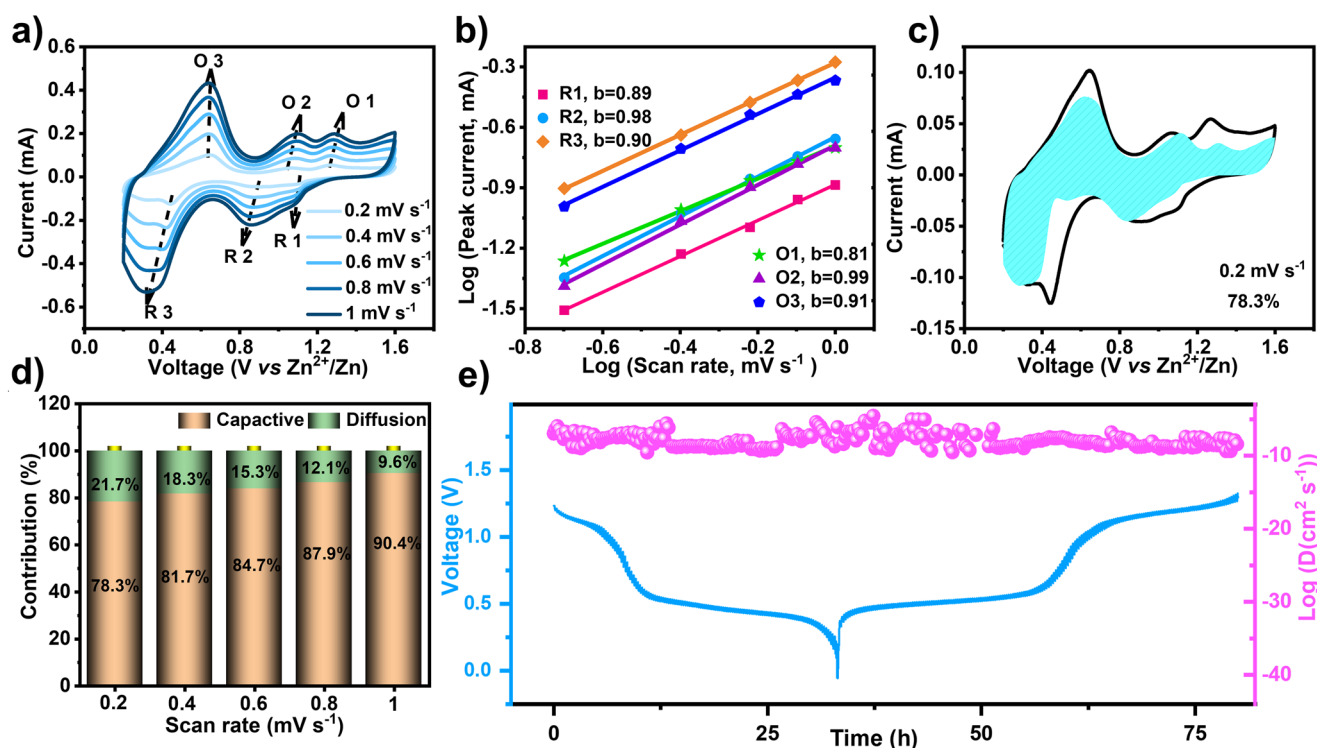
Figure 5. Kinetic analyzes on p-CDs electrodes. a) CV curves of p-CDs at various scan rates from 0.2 to 1 mV s^{-1}, b) log(i) ~ log(v) plots of anodic and cathodic peaks derived from the obtained CV curves. c) Capacitive contribution at a scan rate of 0.2 mV s^{-1}. d) Proportions of the capacitive contribution and the diffusion contribution at different scan rates, respectively. e) GITT curves and diffusion coefficients at a repeating constant current pulse of 30 mA g^{-1}.

the organic electrolytes on the p-CDs cathodes are shown in Figure S12, respectively. Since the orgainc groups on p-CDs are hydrophobic, the p-CDs cathodes exhibit much smaller contact angles toward organic solvents than that in water, which indicate p-CDs are easy to enter the organic electrolyte, and thus, the cathodes are not stable in the organic electrolyte. In the aqueous electrolyte, p-CDs display remarkable cycling capacity, which even retain 90.8% of the original capacity after 1000 cycles at 1 A g^{-1} (Figure 4d).

Moreover, the p-CDs constructed cathode exhibits superior rate performance that its capacity varies from 237 to 103 mAh g^{-1} when the current densities changes from 0.1 to 10 A g^{-1} (Figure 4e), and its capacity can return to 240 mAh g^{-1} as the current density reverts to 0.1 A g^{-1}. With a decent working voltage, a high capacity and a superior rate performance, the specific energy density of p-CDs electrodes is up to 133.3 Wh kg^{-1} that is evaluated on the basis of the cathode materials and the consumed Zn anode, and the corresponding power density can achieve 52.1 W kg^{-1} (Figure 4f). Specifically, the energy density can retain 31 Wh kg^{-1} at an ultrahigh power density of 9322 W kg^{-1}. In addition, long-term cycling stability is investigated at current densities of 5 and 10 A g^{-1} in Figures S13 and 4g, respectively. At a current density of 5 A g^{-1}, the capacity of p-CDs cathode is 126.7 mAh g^{-1} at first, and it retains 115.4 mAh g^{-1} after 5000 cycles, representing a capacity retention ratio of 91.1%. When the stability is examined at a current density of 10 A g^{-1}, the cathode delivers a capacity of 101 mAh g^{-1} over

10 000 cycles, with a capacity retention of 87.4% and a CE of nearly 100%. To the best of our knowledge, p-CDs cathode shows outstanding specific capacities, retention ratios, and cycle numbers among various small molecules, polymers, and inorganic cathode materials for ZIBs (Figure 4h).[29–40]

In order to further investigate the stability of the p-CDs cathode, self-discharge/charge measurements were carried out carefully. After being charged to 1.6 V, the battery shows a stable voltage plateau during a 24 h rest (Figure S14a, b). The discharge capacity after rest is almost the same as the charge capacity. The same results are observed in the self-charge measurement (Figure S14c, d). Thus, the self-discharge/charge is negligible on the fully charged/discharged states. The solubility of p-CDs electrode in 2 M Zn(OTf)$_2$ electrolyte was observed after 50 and 100 days, respectively (Figure S15). There was no p-CDs detected in the electrolyte, by direct observation in daylight and UV light respectively. The electrochemical impedance spectroscopy (EIS) measurements on the Zn∥p-CDs batteries were carried out after different cycles (Figure S16). With the cycles increasing especially after 500 charge/discharge cycles, the R_{ct} remains at around 75 Ω, which also implies the p-CDs electrode has excellent stability.

Reaction kinetics of p-CDs electrode was investigated by CV measurements at various scan rates ranging from 0.2 to 1.0 mV s^{-1}. With the scan rate increases, the CV curves display obviously increased peak currents with similar shapes and slight polarization (Figure 5a). The voltammetry responses of the p-CDs electrode at different scan rates obey

the power-law formula, $i = a\nu^b$, in which i and ν are the peak current and the scan rate, a and b are parameters, respectively. According to the fitted curves in Figure 5b, the b value for peak is more than 0.5, indicating the charge storage of p-CDs is a combination of diffusion and capacitive controlled process. Furthermore, equation $i = k_1\nu + k_2\nu^{1/2}$ was applied to quantitatively calculate the proportions from the diffusion ($k_2\nu^{1/2}$) and the capacitive ($k_1\nu$) contributions, respectively.[41,42] As shown in Figures 5b,d and S17, the capacitive contribution proportion improves from 78.3% to 90.4% as scan rates increasing from 0.2 to 1.0 mV s^{-1}. These results indicate that the charge storage of p-CDs is predominantly based on the nondiffusion-controlled process and thus displays fast reaction kinetics. To investigate the diffusion dynamics, the apparent diffusion coefficients (D) are estimated by the galvanostatic intermittent titration technique (GITT) in Figure 5e. The ion diffusion coefficient could be calculated by the following equation,[43,44]

$$D = \frac{4}{\pi\tau}\left(\frac{V}{S}\right)^2\left(\frac{\Delta E_s}{\Delta E_t}\right)^2$$

where D is the diffusion coefficient, τ is the relaxation time (10 min in this case), V is the volume of the active material, S is the area of the electrode, ΔE_s and ΔE_t are the voltage change caused by the pulse and the charge/discharge processes, respectively. As depicted in Figure 5e, the average ion transport coefficient (D_k) is up to $10^{-8} \sim 10^{-7}$ cm^2 s^{-1}, several orders of magnitude higher than those of the conventional cathode materials (Table S1). This result confirms our p-CDs exhibit outstanding reaction kinetics as cathode materials.

Conclusion

A new type of CDs is synthesized from *o*-phenylenediamine hydrothermally at a large scale, which has conjugated phenazine structure as the reversible redox centers. They can solely severe as the cathode material for aqueous ZIBs and deliver a high specific capacity of 290 mAh g^{-1} at 0.1 A g^{-1}, as well as a lifespan over 10 000 cycles with 87.4% of the capacity retention at 10 A g^{-1}. In situ ATR-FTIR, ex situ XPS, ex situ UV–vis spectra and SEM-mapping studies verify a reversible uptake/removal reaction mechanism for both Zn^{2+} and H$^+$ ions in the p-CDs cathode, where the Zn^{2+} storage is dominant. Moreover, this CDs material exhibits an outstanding ion diffusion coefficient of $10^{-8} \sim 10^{-7}$ cm^2 s^{-1} that is much higher than those of many other organic and inorganic materials for ZIB electrodes. We believe that this work establishes a new way to design full carbon cathodes for the battery storage, which is based on the unique inorganic–organic hybrid structure of CDs.

Conflict of Interests

The authors declare no conflict of interest.

Data Availability Statement

The data that support the findings of this study are available from the corresponding author upon reasonable request.

[1] Q. Cheng, T. Zhang, Q. Wang, X. Wu, L. Li, R. Lin, Y. Zhou, S. Qu, *Adv. Mater.* **2024**, *36*, 2408685.

[2] Y. Ouyang, Y. Biniuri, M. Fadeev, P. Zhang, R. Carmieli, M. Vazquez-Gonzalez, I. Willner, *J. Am. Chem. Soc.* **2021**, *143*, 11510–11519.

[3] J. Chang, W. Jing, X. Yong, A. Cao, J. Yu, H. Wu, C. Wan, S. Wang, G. I. Waterhouse, B. Yang, *Nat. Synth.* **2024**, *3*, 1427–1438.

[4] Z. Zhang, X. Zhou, J. Dong, T. Xue, Y. Di, B. Li, N. Zhao, L. Dai, L. Wang, Z. He, *Adv. Energy Mater.* **2024**, *14*, 2402721.

[5] H. Zhang, S. Li, L. Xu, R. Momen, W. Deng, J. Hu, G. Zou, H. Hou, X. Ji, *Adv. Energy Mater.* **2022**, *12*, 2200665.

[6] F. Liu, S. Xu, W. Gong, K. Zhao, Z. Wang, J. Luo, C. Li, Y. Sun, P. Xue, C. Wang, *ACS Nano* **2023**, *17*, 18494–18506.

[7] M. Shi, H. Zhu, C. Chen, J. Jiang, L. Zhao, C. Yan, *Int. J. Met. Mater.* **2023**, *30*, 25–32.

[8] J. Li, P. Guo, G. Chen, C. Wu, Y. Xiao, H. Dong, Y. Liang, Y. Liu, H. Hu, M. Zheng, *J. Energy Stor* **2024**, *84*, 110632.

[9] B.-H. Xu, Y.-H. Song, G.-D. Yang, J.-Y. Zhang, Y.-Q. Liu, J.-Q. Liu, Q.-M. Zhang, X.-L. Wu, M.-X. Deng, H.-Z. Sun, *Chem. Eng. J.* **2024**, *499*, 156341.

[10] Y. Xue, H. Zhou, Z. Ji, X. Shen, J. Cao, J. Pu, L. Kong, A. Yuan, *Appl. Surf. Sci.* **2023**, *633*, 157580.

[11] C. Xia, J. Zhong, X. Han, S. Zhu, Y. Li, H. Liu, B. Yang, *Angew. Chem. Int. Ed.* **2024**, *63*, e202410519.

[12] Y. Shen, C. Luo, C. Chen, X. Zhang, M. Shi, Z. Gu, R. Su, Y. Wang, L. Li, L. Wang, *Adv. Mater.* **2024**, *37*, 2407811.

[13] L. Tang, H. Peng, J. Kang, H. Chen, M. Zhang, Y. Liu, D. H. Kim, Y. Liu, Z. Lin, *Chem. Soc. Rev.* **2024**, *53*, 4877–4925.

[14] Y. Liu, L. Wu, *Nano Energy* **2023**, *109*, 108290.

[15] Y. Zhang, S. Lu, *Chem* **2024**, *10*, 134–171.

[16] M. Vedamalai, A. P. Periasamy, C.-W. Wang, Y. T. Tseng, L.-C. Ho, C.-C. Shih, H.-T. Chang, *Nanoscale* **2014**, *6*, 13119–13125.

[17] J. Liu, T. Kong, H. M. Xiong, *Adv. Mater.* **2022**, *34*, 2200152.

[18] L. Cao, M. Zan, F. Chen, X. Kou, Y. Liu, P. Wang, Q. Mei, Z. Hou, W.-F. Dong, L. Li, *Carbon* **2022**, *194*, 42–51.

[19] J. S. Wei, C. Ding, P. Zhang, H. Ding, X. Q. Niu, Y. Y. Ma, C. Li, Y. G. Wang, H. M. Xiong, *Adv. Mater.* **2019**, *31*, 1806197.

[20] N. Soni, S. Singh, S. Sharma, G. Batra, K. Kaushik, C. Rao, N. C. Verma, B. Mondal, A. Yadav, C. K. Nandi, *Chem. Sci.* **2021**, *12*, 3615–3626.

[21] M. Niu, F. Zheng, X. Yang, P. Bi, L. Feng, X. Hao, *Org. Electron.* **2017**, *49*, 340–346.

[22] L. Ma, K. Zhang, C. Kloc, H. Sun, M. E. Michel-Beyerle, G. G. Gurzadyan, *Phys. Chem. Chem. Phys.* **2012**, *14*, 8307.

[23] Z. Li, M. Zhang, L. Zhang, X. Dong, L. Leng, J. H. Horton, J. Wang, *Nano Res.* **2022**, *15*, 1338–1346.

[24] C. Ye, X. Zhou, S. Tang, *Angew. Chem. Int. Ed.* **2025**, *64*, e202501743.

[25] L. Lin, Z. Lin, J. Zhu, K. Wang, W. Wu, T. Qiu, X. Sun, *Energy Environ. Sci.* **2023**, *16*, 89–96.

[26] Y. Chen, J. Li, Q. Zhu, K. Fan, Y. Cao, G. Zhang, C. Zhang, Y. Gao, J. Zou, T. Zhai, C. Wang, *Angew. Chem. Int. Ed.* **2022**, *61*, e202116289.

[27] Y. Zhang, M. Li, Z. Li, Y. Lu, H. Li, J. Liang, X. Hu, L. Zhang, K. Ding, Q. Xu, *Angew. Chem. Int. Ed.* **2024**, *136*, e202410342.

[28] W. Wang, V. S. Kale, Z. Cao, Y. Lei, S. Kandambeth, G. Zou, Y. Zhu, E. Abouhamad, O. Shekhah, L. Cavallo, *Adv. Mater.* **2021**, *33*, 2103617.

[29] Y. An, Y. Liu, S. Tan, F. Xiong, X. Liao, Q. An, *Electrochim. Acta* **2022**, *404*, 139620.

[30] W. Wang, V. S. Kale, Z. Cao, S. Kandambeth, W. Zhang, J. Ming, P. T. Parvatkar, E. Abou-Hamad, O. Shekhah, L. Cavallo, M. Eddaoudi, H. N. Alshareef, *ACS Energy Lett.* **2020**, *5*, 2256–2264.

[31] G. Li, Z. Yang, Y. Jiang, C. Jin, W. Huang, X. Ding, Y. Huang, *Nano Energy* **2016**, *25*, 211–217.

[32] Y. Zeng, X. F. Lu, S. L. Zhang, D. Luan, S. Li, X. W. Lou, *Angew. Chem. Int. Ed.* **2021**, *60*, 22198–22194.

[33] S. Zheng, D. Shi, D. Yan, Q. Wang, T. Sun, T. Ma, L. Li, D. He, Z. Tao, J. Chen, *Angew. Chem. Int. Ed.* **2022**, *61*, e202117511.

[34] H. Sun, L. Yang, E. Hu, M. Feng, C. Fan, W. Wang, H. Li, X. Wang, Z. Liu, *ACS App. Mater. Inter.* **2022**, *14*, 40247–40256.

[35] S. Li, Y. Liu, X. Zhao, Q. Shen, W. Zhao, Q. Tan, N. Zhang, P. Li, L. Jiao, X. Qu, *Adv. Mater.* **2021**, *33*, 2007480.

[36] X. Liu, G. Xu, Q. Zhang, S. Huang, L. Li, X. Wei, J. Cao, L. Yang, P. K. Chu, *J. Power Sources* **2020**, *463*, 228223.

[37] Q. Wang, T. Sun, S. Zheng, L. Li, T. Ma, J. Liang, *Inorg. Chem. Front.* **2021**, *8*, 4497–4506.

[38] H. Zhang, Y. Fang, F. Yang, X. Liu, X. Lu, *Energy Environ. Sci.* **2020**, *13*, 2515–2523.

[39] H. Lu, J. Hu, K. Zhang, J. Zhao, S. Deng, Y. Li, B. Xu, H. Pang, *Adv. Mater.* **2024**, *36*, 2309753.

[40] T. Sun, W. Zhang, Z. Zha, M. Cheng, D. Li, Z. Tao, *Energy Storage Mater.* **2023**, *59*, 102778.

[41] L. Yan, Q. Zhu, Y. Qi, J. Xu, Y. Peng, J. Shu, J. Ma, Y. Wang, *Angew. Chem. Int. Ed.* **2022**, *61*, e202211107.

[42] X. Wu, Y. Xu, C. Zhang, D. P. Leonard, A. Markir, J. Lu, X. Ji, *J. Am. Chem. Soc.* **2019**, *141*, 6338–6344.

[43] S. Guo, S. Liang, B. Zhang, G. Fang, D. Ma, J. Zhou, *ACS Nano* **2019**, *13*, 13456–13464.

[44] X. Geng, H. Ma, F. Lv, K. Yang, J. Ma, Y. Jiang, Q. Liu, D. Chen, Y. Jiang, N. Zhu, *Chem. Eng. J.* **2022**, *446*, 137289.